EXPLORATION OF STRUCTURAL, ELECTRONIC, AND MAGNETIC CHARACTERISTICS OF XYZ HALF-HEUSLER COMPOUNDS THROUGH THE TB-LMTO METHOD

Abstract

Employing the Tight-Binding Linear Muffin-Tin Orbital (TBLMTO) approach, we delve into the structural, electronic, and magnetic attributes of XYZ (where X includes Li, Na, K, and Rb; Y encompasses Mg, Ca, Sr, and Ba; and Z pertains to C, Si, Ge, and Sn) compounds structured within the half-Heusler framework. The investigation encompasses the computation of ground-state characteristics, such as lattice parameters and bulk modulus, achieved via total energy calculations rooted in the Tight-Binding Linear Muffin-Tin Orbital (TBLMTO) method. Our results from spin-polarized calculations reveal that a significant number of compounds studied exhibit the desirable half-metallic ferromagnetic (HMF) property, with an integer magnetic moment of 1.0 μ_B per formula unit at their equilibrium volume. The origin of the magnetic moment is found to be primarily associated with the p-like states of Z atoms. Moreover, the half-metallicity is observed over a wide range of lattice constants, making these half-Heusler alloys highly intriguing for potential applications in the field of spintronics.

Keywords: Half-Heusler alloys, TBLMTO calculations, Spintronics materials, Magnetic properties, electronic band structure.

Authors

R. Umamaheswari
Department of Physics
Anna University
Chennai, India.
mahi77.r@gmail.com

G. Kalpana
Department of Physics
Anna University
Chennai, India.

G. Jaiganesh
Excel Instruments
Dias Industrial Estate
Vasai East
Sativali Naka
Maharastra, India.

I. INTRODUCTION

The realm of spintronics has experienced a notable upswing in scholarly attention, driven by the quest for novel materials boasting substantial spin polarization. Such advancements are pivotal in harnessing the complete capabilities of spintronic devices [1]. Among the promising candidates, half-metallic ferromagnets (HMF) have emerged as compelling materials with exceptional electronic structures, offering the ideal characteristics for spintronics applications. These substances showcase metallic tendencies concerning one electron spin, while manifesting insulating or semiconducting traits in relation to the other spin, culminating in a 100% spin-polarized electronic density of states at the Fermi level. The notion of half metallicity was initially theorized by de Groot et al. [2], initially observed in the instance of the half-Heusler compound NiMnSb. Subsequently, a multitude of studies have delved into the potential for Half Metallic Ferromagnetism (HMF) in various materials, encompassing ferromagnetic metallic oxides [3-4], Heusler compounds [5-6], diluted magnetic semiconductors [7-8], binary transition metal pnictides [9], and chalcogenides possessing zinc-blende (ZB) structures [10].

Heusler alloys, with both full-Heusler (X_2YZ) and half-Heusler (XYZ) compositions, have drawn considerable attention as potential HMF materials. The half-Heusler compounds, in particular, present unique merits in comparison to alternative materials, showcasing elevated Curie temperatures and favorable lattice compatibility with wide bandgap semiconductors like GaAs. The Heusler compound class was initially identified by Heusler in 1903, featuring full-Heusler compounds that crystallize within the L21 structure, and half-Heusler compounds that take form in the C1b structure. In these compounds, the X and Y sites are inhabited by transition metals, while the Z sites are occupied by main group elements [11]. Comprehensive explorations, encompassing both theoretical and empirical investigations, have been carried out on both full-Heusler and half-Heusler compounds. Within these studies, a considerable number have been anticipated to manifest Half Metallic Ferromagnetism (HMF) attributes [12-16].

Recently, a novel category of materials has come to light, characterized by the absence of transition metals, yet retaining the capacity to achieve spin polarization. These d^0 or sp HMF materials, as they are known, owe their spin-polarization to the presence of anion p-like electrons, making them promising candidates for spintronics applications. Geshi et al. [17] and Kusakabe et al. [18] were among the first to predict HMF behavior in certain sp materials, such as CaP, CaAs, and CaSb, in zinc-blende structures. Follow-up investigations have delved into the electronic and magnetic characteristics of compounds involving alkali metals and alkaline earth metals paired with main group (sp) elements. These inquiries have unveiled additional prospects for materials that could exhibit Half Metallic Ferromagnetism (HMF) [19-26].

Limited research has been conducted on the ferromagnetic properties of half-Heusler alloys without any transition metals. Chen et al. [27] predicted that GeKCa and SnKCa exhibit Half Metallic Ferromagnetism (HMF) in the half-Heusler structure. Magnetic properties of RbSrX and XCsBa (X = C, Si, and Ge), as well as LiCaC and NaCaC compounds, have been examined by Rozale et al. [28], Lakdja et al. [29], and Umamaheswari et al. [30], respectively. These investigations revealed that these materials display HMF with

an integer magnetic moment of $1\mu_B$. These studies have intensified our research interest in the quest for new HMF materials within the half-Heusler structure without any transition metals.

Within this context, the primary objective of this paper revolves around the exploration of the electronic structure and magnetic attributes of hypothetical XYZ compounds structured within the half-Heusler framework. This endeavour is carried out using the Tight-Binding Linear Muffin-Tin Orbital (TBLMTO) method. Distinguishing itself from prior inquiries, this study delves into the stability of the ferromagnetic (FM) state via both spin-polarized and spin-unpolarized calculations.

Through a systematic analysis of the properties inherent in these materials, our aim is to discern potential half-Heusler alloys devoid of transition metals yet showcasing Half Metallic Ferromagnetism (HMF) tendencies. The subsequent sections will delve into the computational particulars (Section II), present the outcomes of our calculations and their corresponding discussions (Section III), and culminate in concluding remarks (Section IV).

II. COMPUTATIONAL METHODOLOGY

We are investigating the structural, electronic, and magnetic properties of XYZ compounds, where X represents Li, Na, K, and Rb; Y includes Mg, Ca, Sr, and Ba; and Z encompasses C, Si, Ge, and Sn. To carry out this investigation, we are using the tight-binding linear muffin-tin orbital (TB-LMTO) method within the atomic-sphere approximation (ASA). The TB-LMTO method was initially proposed by Andersen [31] and later refined by Andersen and Jepsen [32]. It involves accurately transforming Andersen's linear muffin-tin orbitals into localized, short-range, or tight-binding orbitals. This method has gained widespread application in materials research due to its precision in describing the electronic structure and properties of intricate systems.

The potential is computed within the local spin density approximation (LSDA), utilizing the parameterization scheme as developed by von Barth and Hedin [33]. Additionally, combined correction terms are introduced to accommodate non-spherical shapes of atomic cells and the truncation of higher partial waves ($l > 2$) within the spheres. These corrections play a crucial role in mitigating errors within the TB-LMTO method, ensuring a robust representation of the electronic properties inherent in the compounds under investigation.

To maintain the crystal symmetry while upholding accuracy, vacant spheres are introduced strategically to achieve close packing. In this calculation, the maximum overlap between atomic spheres is limited to around 16%, ensuring an optimal portrayal of electronic states within the system.

For integrating across the Brillouin zone (k space), the tetrahedron method is utilized in its latest iteration. This version effectively avoids miscalculations and rectifies errors stemming from linear approximations of bands within each tetrahedron [34]. A grid of 16×16×16 points is employed in the irreducible part of the Brillouin Zone, guaranteeing well-converged outcomes. Both energy (E) and wave vector (k) convergence are meticulously verified to establish the credibility of the computed properties.

The scalar-relativistic approximation is adopted, encompassing all relativistic effects except for spin-orbit coupling. This selection permits us to focus on the fundamental electronic and magnetic traits of the XYZ compounds, bypassing the computational complexity introduced by integrating spin-orbit coupling.

By implementing the TB-LMTO method with these specified computational parameters and including essential correction terms, our aim is to achieve a comprehensive grasp of the structural, electronic, and magnetic features characterizing the XYZ compounds within the half-Heusler structure.

III. RESULTS AND DISCUSSION

1. **Structural Properties:** In essence, half-Heusler phases are cubic ternary intermetallic compounds represented by the general formula XYZ. These compounds adopt a non-centrosymmetric cubic MgAgAs (C1b) structure, falling under the F-43m space group. This structure consists of three interwoven face-centered cubic (fcc) lattices of X, Y, and Z atoms, positioned at coordinates r1 = (0.5, 0.5, 0.5), r2 = (0, 0, 0), and r3 = (0.25, 0.25, 0.25) relative to the cubic lattice's constant unit, 'a'. Half-Heusler phases are derived from the true Heusler phases X_2YZ by the removal of one X atom, resulting in a vacant site. This specific structural arrangement is upheld through covalent bonding, involving the transfer of s electrons from the X and Y metals to the p shell of the Z element. Extensive literature expounds upon the crystalline configuration (C1b) as well as various atomic arrangements (α, β, γ-phases) within this structure [35-39].

   To establish the most stable phase among the three distinct phases (α, β, γ-phases) within the C1b-type structure of XYZ compounds, the initial step involves computing total energy values as a function of the unit cell volume. The findings indicate that, in comparison to the β and γ-phases, all compounds are notably more stable in the α-phase. Consequently, our focus narrows down exclusively to the α-phase. In order to investigate the potential for ferromagnetism within these compounds, we conduct calculations in both spin-polarized (FM) and spin-unpolarized (NM) modes for all compounds within the α-phase. As illustrated in Fig. 1(a) and (b) for the LiSrSi compound, it becomes evident that, for most compounds, the FM state boasts lower energy than the NM state. This observation suggests that the FM state holds greater stability.

   The equilibrium lattice parameter is determined by fitting the total energy concerning volume to the Birch equation of state [40]. The anticipated lattice parameters, bulk moduli, and the discrepancies in total energy (spin-polarization energy, $\Delta E = E_{NM} - E_{FM}$) between the spin-unpolarized (NM) and spin-polarized (FM) states are itemized in Table 1 (a-d), along with existing theoretical outcomes. The computed lattice constants show a minor underestimation, and the bulk moduli are somewhat overestimated in contrast to other theoretical values [27, 28].

   This variation can be attributed to the utilization of the local density approximation (LDA) in contrast to other approximations (such as GGA) employed in alternative studies. The lattice parameter enlarges as the atomic number increases, moving from X = Li to Rb, Y = Mg to Ba, and Z = C to Sn. A positive value for ΔE indicates that the FM state is energetically more stable compared to the NM state, while

$\Delta E = 0$ signifies a lack of spin polarization in energy states around the Fermi level. Based on the table, it becomes evident that compounds like LiMgZ (Z = C, Si, Ge, and Sn), LiBaC, NaBaC, KMgSn, NaMgZ, and XBaZ (X = Li, Na, K, and Rb; Z = Si, Ge, and Sn) exhibit non-magnetic behavior ($\Delta E = 0$). Conversely, other compounds within this series exhibit ferromagnetic traits (ΔE = positive value).

Before investigating the electronic and magnetic properties, it is essential to calculate the formation energy of these hypothetical compounds, which indicates their stability with respect to decomposition into bulk constituents. The formation energy (ΔH) is calculated using the following expression,

$$\Delta H = \frac{1}{a+b+c}\left[E^{XYZ}_{Total} - aE^{X}_{Solid} - bE^{Y}_{Solid} - cE^{Z}_{Solid}\right]$$

Where, E^{XYZ}_{Total} refers to the total energy of the crystal or primitive cell used in the present calculations and *a*, *b* and *c* refer to the number of X, Y and Z atom respectively. E^{X}_{solid}, E^{Y}_{solid} and E^{Z}_{solid} are the total energy of the pure elemental constituents.

The computed heat of formation (ΔH) is outlined in Table 1 (a-d), where a negative value signifies that the mentioned compounds will remain intact and not break apart once they are formed. This finding provides additional evidence of their stability. The cubic MgAgAs-type structure of the XYZ half-Heusler compounds, characterized by their varied atomic arrangements, undergoes thorough analysis, leading to the identification of the stable α-phase for comprehensive exploration.

The presence of ferromagnetism is evaluated through both spin-polarized and spin-unpolarized calculations, allowing us to uncover the magnetic attributes of these compounds. Furthermore, the computed lattice parameters, bulk moduli, and formation energies offer crucial insights into the structural stability and electronic characteristics of these captivating materials.

2. **Electronic and Magnetic Characteristics:** Spin-polarized calculations of band structures and density of states (DOS) are conducted for all compounds using their equilibrium lattice parameters. Because of the similarity in their electronic structures, representative band structures are shown for compounds that exhibit non-magnetic (NM), half-metallic ferromagnetic (HMF), and nearly HMF behavior. This is demonstrated through illustrative band structures for LiMgC, LiSrSi, and RbSrSi compounds, as depicted in Figure 2 (a-c).

From Figure 2 (a), it is evident that the compounds LiMgZ (Z = C, Si, Ge, and Sn), LiBaC, NaBaC, KMgSn, NaMgZ, and XBaZ (X = Li, Na, K, and Rb; Z = Si, Ge, and Sn) exhibit non-magnetic behavior (NM). This is characterized by the absence of spin-polarization of energy states around the Fermi level (E_F), and both spin channels exhibit metallic behavior with no magnetic moment.

In contrast, when delving into spin-polarized calculations for the remaining compounds-namely, XMgC (X = Na - Rb), XMgZ (X = K, Rb; Z = Si, Ge), RbMgSn, XCaZ, and XSrZ (X = Li - Rb; Z = C - Sn) -distinct spin-splitting of energy states near the Fermi level comes to the forefront. This signifies the presence of ferromagnetism (FM) within these compounds. Moreover, in the majority of compounds manifesting ferromagnetism (with exceptions being LiCaSn, RbSrZ (Z = Si, Ge, and Sn), and RbCaGe), the minority spin channel exhibits metallic behavior, while the majority spin channel demonstrates a semiconducting characteristic with an energy gap around the Fermi level (as depicted in Fig. 2 (b)). As a result, these compounds epitomize the traits of half-metallic ferromagnetic (HMF) behavior, featuring an integer magnetic moment of $1\mu_B$ - a distinctive hallmark of HMFs.

The cumulative magnetic moment follows the principles of Slater-Pauling behavior, which interconnects the total number of valence electrons and the overall spin magnetic moments within half-metallic alloys. Within the mentioned XYZ systems, $N\downarrow$ equals 3, and Z_t equals 7, ultimately yielding a total magnetic moment of $M_t = 1\mu_B$.

In Figure 2 (b), it can be observed that the top of the majority-spin valence band slightly crosses the Fermi level, indicating metallic behavior in both spin channels. The same trend is observed in LiCaSn, RbCaGe, and RbSrZ (Z = Ge and Sn) compounds. Despite spin-splitting around the Fermi level, the metallic behavior in both channels suggests the absence of HMF property at their equilibrium volume, and the calculations show that these compounds have a non-integer magnetic moment, making them FM and metallic in nature.

To determine the HM (half-metallic) gap and majority spin band gap, the band structure of LiSrSi is discussed here for clarity (Fig. 2(b)). It can be observed that the top of the majority-spin valence band is at 0.30 eV, and the majority-spin conduction bands are at 1.17 eV. The spin-flip gap or HM gap is the minimum of these two values, and for LiSrSi, the HM gap is 0.30 eV. The HM gap (EHM) and majority spin band gap ($E_g\uparrow$) for the mentioned compounds are listed in Table 2 (a-d), and these values are slightly smaller when compared with available theoretical values [27, 28].

This discrepancy is due to the use of LSDA, which delocalizes the electrons more compared to GGA-PBE exchange correlation. The non-zero HM gaps for these compounds (Table 2(a-d)) confirm their true HMF nature. Additionally, it is observed that the majority spin band gap becomes smaller as we move along the 4^{th} column (C → Si → Ge → Sn) of the periodic table.

To comprehend the source of the magnetic moment, the spin-polarized total and partial density of states (DOS) for all compounds are computed at their equilibrium lattice constants. The overall DOS pattern for XYZ compounds remains consistent, and for illustrative purposes, the spin-dependent total and partial DOS for LiSrSi are depicted in Figure 3. A comparison between the partial DOS and the band structure diagram (Fig. 2(b)) reveals that the lower band corresponds to the anion's (Si) 2s-like states.

The subsequent band adjacent to the Fermi level represents a fusion of the anion's 2p-like states with the cation's (Sr) 4d and 4s-like states, along with the cation's (Li) 2s-

like state. In the minority spin channel, the anion's 2p-like states are partially occupied, leading to a crossing of the Fermi level and showcasing metallic attributes. In contrast, the majority spin channel features the anion's 2p-like states fully occupied with three electrons, positioning them within the valence band and displaying semiconductor characteristics. This phenomenon gives rise to a 100% spin-polarization of energy states encircling the Fermi level, engendering the occurrence of HMF behavior. Furthermore, it's evident that the band near the Fermi level primarily stems from the anion's 2p-like states. This band demonstrates substantial spin-polarization around the Fermi level due to the interplay between the anion's 2p-like state and the cation's (Sr) 4d-like state. Thus, the magnetic moment in this compound is predominantly rooted in the anion's 2p-like states, with a calculated magnetic moment of 1.0 μB per formula unit.

The electronic arrangement of XYZ compounds finds its basis in their seven valence electrons: X (ns1), Y (ns2), and Z (ns2, np2). In this setup, X and Y atoms contribute their ns state electrons to Z-np states. In terms of energy, the low bands positioned around -6 eV below the Fermi level within both the majority-spin and minority-spin channels (as shown in Fig. 2(b)) are populated by the two valence electrons originating from ns-like states of Z. Additionally, three valence electrons effectively fill up the three majority-spin bands in proximity to the Fermi level, whereas the remaining two electrons partly occupy the corresponding three minority-spin bands.

This distribution results in a single vacancy, leading to a cumulative magnetic moment of 1μB for every formula unit. The precise total and partial magnetic moments are detailed in Table 2 (a-d), showcasing that the primary contributor to the overall magnetic moment stems from the p-like states of the anion (Z) atom. The magnetic moment of the other atoms is relatively minor. This effect arises from the interaction between the p-like states of the anion and d-like states of the cation (Y). Within these compounds, the unpaired electrons reside within clearly defined states, attributing magnetism to localized electrons.

The compounds LiCaSn, RbCaGe, and RbSrZ (Z = Si, Ge, and Sn) are FM and metallic in nature at their equilibrium volume and exhibit HMF properties at an expanded volume. For example, the spin-polarized total DOS of RbSrGe at its optimized and expanded volumes are shown in Fig. 4(a & b). From these figures, it is observed that at its expanded volume, there is a semiconducting gap in the majority spin channel and band overlap in the minority spin channel.

This indicates that at their expanded volume, spin-splitting occurs around the Fermi level, and true HMF with 1.0 μ_B appears when their volume becomes large enough. However, at their equilibrium volume, even though there is spin-polarization around the Fermi level, it exhibits nearly HMF properties by having a non-integer magnetic moment. The calculated lattice constant (a_{ex}) where the HMFs exist at an expanded volume, total magnetic moment, half-metallic gap, and majority spin gap for LiCaSn, RbSrZ (Z = Si, Ge, and Sn), and RbCaGe compounds at their expanded volume are given in Table 3.

In the titled compounds, mainly the compounds containing Ca and Sr show the HMF property due to the presence of unoccupied 3d and 4d states of Ca and Sr, which are close in energy to the occupied p-like states of the Z atom. As a result, p-d hybridization

is strong enough when compared to the situation in Mg, where the 3d states are much higher in energy. Additionally, in Ba-based compounds, 4f bands occur in the unoccupied states when compared to 3d and 4d states of Ca and Sr.

Therefore, in Mg and Ba-based compounds, p-d hybridization is very weak, and the spin-splitting around the Fermi level is also very small. Consequently, most Mg and Ba-based compounds in the mentioned XYZ series are non-magnetic.

The comprehensive findings regarding the electronic and magnetic attributes of XYZ compounds are consolidated in Table 4. A '-' symbol is used to denote non-magnetic and metallic systems, a '+' symbol signifies half-metallic ferromagnetism (HMF) at the equilibrium volume, and 'Δ' indicates HMF behavior at the expanded volume.

3. **Durability of Half-Metallicity:** To determine the durability of half-metallicity, it's pivotal to explore how the total magnetic moment changes with alterations in the lattice constant. This examination is carried out for the aforementioned half-metallic compounds. As an example, Fig. 5 illustrates how the total magnetic moment shifts as the lattice constant varies for XCaC and XSrC (X = Li-Rb) compounds. Notably, it can be observed that the total magnetic moment remains constant until the lattice constant is compressed to a specific critical value, showcasing a characteristic of strong half-metallicity.

   The respective critical lattice constant values are detailed in Table 2(a-d). This pattern indicates the resilience of half-metallicity, as it remains robust across a range of lattice constants for these compounds. In conclusion, the exploration of how the total magnetic moment changes with lattice constant contraction corroborates the steadfast nature of half-metallicity within the compounds under scrutiny. This robustness is of significance, as it suggests that these materials uphold their half-metallic ferromagnetic characteristics when subjected to certain compressive strain conditions.

IV. CONCLUSION

In summary, our investigation has been centered around the exploration of new half-metallic ferromagnetic materials (HMFs) that do not rely on the presence of transition metals. We have conducted a systematic study of the electronic structure and magnetic attributes of XYZ compounds (where X ranges from Li to Rb; Y includes Mg to Ba; and Z covers C to Sn) within the half-Heusler structure, utilizing the TB-LMTO method.

Our consistent total-energy calculations have consistently demonstrated that the ferromagnetic (FM) state is more energetically favored than the non-magnetic (NM) state for most compounds within this series. Furthermore, the negative values of the formation energy for these compounds underscore their intrinsic stability, suggesting that they are unlikely to break apart once they form.

Through detailed spin-polarized calculations, we have identified several compounds that exhibit the coveted half-metallic ferromagnetic properties. Compounds like XMgC (X = Na - Rb), RbMgSn, XMgZ, XBaC (X = K, Rb; Z = Si, Ge), XCaZ, XSrC (X = Li - Rb; Z = C, Si), XCaGe, XSrZ (X = Li - K; Z = Si - Sn), and XCaSn (X = Na - Rb) display this

behavior, featuring substantial half-metallic gaps (with values reaching up to 0.536 eV for LiCaC). The calculated total magnetic moment of 1μB per formula unit mainly stems from the localized p-like states of the Z atoms.

The substantial half-metallic gaps, coupled with the persistence of half-metallicity even under lattice compression, position these compounds as highly promising candidates for potential spintronics applications. They offer the advantage of efficient spin-polarized current transport, holding significant potential for spintronic devices and technologies. The robustness of their half-metallic properties, even when the lattice is compressed, further enhances their practicality and suitability across diverse spintronics applications.

Our findings contribute to the quest for novel half-metallic ferromagnetic materials devoid of transition metals, broadening the pool of potential candidates for applications in spintronics. This advancement serves to propel the field of materials science and technology forward.

REFERENCES

[1] I. Žutić, J. Fabian, S. D. Sarma, "Spintronics: Fundamentals and applications," Rev. Mod. Phys. 76, 323 (2004).
[2] R. De Groot, F. Mueller, P. Van Engen, K. Buschow, "New class of materials: Half-metallic ferromagnets," Phys. Rev. Lett. 50, 2024-2027 (1983).
[3] Y. S. Dedkov, U. Rüdiger, G. Güntherodt, "Evidence for the half-metallic ferromagnetic state of Fe3O4 by spin-resolved photoelectron spectroscopy," Phys. Rev. B 65, 064417 (2002).
[4] S. P. Lewis, P. B. Allen, T. Sasaki, "Band structure and transport properties of CrO2," Phys. Rev. B 55, 10253 (1997).
[5] S. Picozzi, A. Continenza, A. Freeman, "Co2MnX (X= Si, Ge, Sn) Heusler compounds: An ab initio study of their structural, electronic, and magnetic properties at zero and elevated pressure," Phys. Rev. B 66, 094421 (2002).
[6] A. Kellou, N. Fenineche, T. Grosdidier, H. Aourag, C. Coddet, "Structural stability and magnetic properties in X2AlX′(X= Fe, Co, Ni; X′= Ti, Cr) Heusler alloys from quantum mechanical calculations," J. Appl. Phys. 94, 3292-3298 (2003).
[7] L. Kronik, M. Jain, J. R. Chelikowsky, "Electronic structure and spin polarization of MnxGa1-xN," Phys. Rev. B 66, 041203 (2002).
[8] H. Akai, "Ferromagnetism and its stability in the diluted magnetic semiconductor (In, Mn)As," Phys. Rev. Lett. 81, 3002 (1998).
[9] E. Şaşioglu, I. Galanakis, L. Sandratskii, P. Bruno, "Stability of ferromagnetism in the half-metallic pnictides and similar compounds: a first-principles study," J. Phys. Condens. Matter 17, 3915 (2005).
[10] W.-H. Xie, Y.-Q. Xu, B.-G. Liu, D. Pettifor, "Half-metallic ferromagnetism and structural stability of zincblende phases of the transition-metal chalcogenides," Phys. Rev. Lett. 91, 037204 (2003).
[11] I. Galanakis, P. Mavropoulos, "Spin-polarization and electronic properties of half-metallic Heusler alloys calculated from first principles," J. Phys. Condens. Matter 19, 315213 (2007).
[12] E. Shreder, S. Streltsov, A. Svyazhin, A. Makhnev, V. Marchenkov, A. Lukoyanov, H. Weber, "Evolution of the electronic structure and physical properties of Fe2MeAl (Me= Ti, V, Cr) Heusler alloys," J. Phys. Condens. Matter 20, 045212 (2008).
[13] T. Block, M. Carey, B. Gurney, O. Jepsen, "Band-structure calculations of the half-metallic ferromagnetism and structural stability of full- and half-Heusler phases," Phys. Rev. B 70, 205114 (2004).
[14] K. Özdogan, I. Galanakis, E. Şaşioglu, B. Aktaş, "Search for half-metallic ferrimagnetism in V-based Heusler alloys Mn2VZ (Z= Al, Ga, In, Si, Ge, Sn)," J. Phys. Condens. Matter 18, 2905 (2006).
[15] B. Nanda, I. Dasgupta, "Electronic structure and magnetism in half-Heusler compounds," J. Phys. Condens. Matter 15, 7307 (2003).
[16] H. Luo, Z. Zhu, G. Liu, S. Xu, G. Wu, H. Liu, J. Qu, Y. Li, "Ab-initio investigation of electronic properties and magnetism of half-Heusler alloys XCrAl (X= Fe, Co, Ni) and NiCrZ (Z= Al, Ga, In)," Physica B: Condensed Matter 403, 200-206 (2008).

[17] M. Geshi, K. Kusakabe, H. Nagara, N. Suzuki, "Synthetic ferromagnetic nitrides: First-principles calculations of CaN and SrN," Phys. Rev. B 76, 054433 (2007).
[18] K. Kusakabe, M. Geshi, H. Tsukamoto, N. Suzuki, "New half-metallic materials with an alkaline earth element," J. Phys. Condens. Matter 16, S5639 (2004).
[19] G. Gao, K. Yao, E. Şaşıoğlu, L. Sandratskii, Z. Liu, J. Jiang, "Half-metallic ferromagnetism in zinc-blende CaC, SrC, and BaC from first principles," Phys. Rev. B 75, 174442 (2007).
[20] G. Gao, K. Yao, "Half-metallic sp-electron ferromagnets in rocksalt structure: The case of SrC and BaC," Appl. Phys. Lett. 91, 082512 (2007).
[21] C. -W. Zhang, "Half-metallic ferromagnetism in the zinc-blende MC (M= Li, Na and K)," J. Phys. D: Appl. Phys. 41, 085006 (2008).
[22] C.-W. Zhang, S.-S. Yan, "Half-metallic ferromagnetism in wurtzite MC (Ca, Sr, Ba and Mg)," Solid State Commun. 149, 387-392 (2009).
[23] E. Yan, "Half-metallic properties in rocksalt and zinc-blende MN (M = Na, K): A first-principles study," Physica B: Condensed Matter 407, 879-882 (2012).
[24] M. Moradi, M. Rostami, M. Afshari, "Half-metallic ferromagnetism in Wurtzite MS (M= Li, Na, and K)," Can. J. Phys. 90, 531-536 (2012).
[25] G. Jaiganesh and G. Kalpana, "First-principles study of structural, electronic and magnetic properties of AeX (Ae = Be, Mg, Sr, Ba; X = Si, Ge, and Sn) compounds." Journal of magmetism and magnetic materials, 326, 66-74 (2013).
[26] G.Jaiganesh, R.D. Ethiraj, G.Kalpana and M.Rajagopalan, "Ab-initio band structure calculations of half-metallic calcium pnictides, Physica Status Solidi (b), 244(12),4643-4650,(2007)
[27] J. Chen, G. Gao, K. Yao, M. Song, "Half-metallic ferromagnetism in the half-Heusler compounds GeKCa and SnKCa from first-principles calculations," J. Alloys Compd. 509, 10172-10178 (2011).
[28] H. Rozale, A. Amar, A. Lakdja, A. Moukadem, A. Chahed, "Half-metallicity in the half-Heusler RbSrC, RbSrSi and RbSrGe compounds," J. Magn. Magn. Mater. (2013).
[29] A. Lakdja, H. Rozale, A. Chahed, O. Benhelal, "Ferromagnetism in the half-Heusler XCsBa compounds from first-principles calculations (X = C, Si, and Ge)," J. Alloys Compd. (2013).
[30] R. Umamaheswari, D.Vijayalakshmi and G. Kalpana, "First Principle calculations of structural, electronic and magnetic properties of half-Heusler LiCaC and NaCaC compounds, " Physica B, Condensed matter,448, 256-259 (2014).
[31] H. L. Skriver, "The LMTO Method," Springer, Heidelberg (1984).
[32] O. K. Anderson and O. Jepsen, "Explicit, First-Principles Tight-Binding Theory," Phys. Rev. Lett. 53, 2571-2574 (1984).
[33] V. von Barth and L. Hedin, "A Local Exchange-Correlation Potential for the Spin Polarized Case," J. Phys. C: Solid State Phys. 5, 1629-1642 (1972).
[34] O. Jepsen and O. K. Anderson, "The Electronic Structure of h.c.p Ytterbium," Solid State Commun. 9, 1763-1767 (1971).
[35] A. E. Carlsson, A. Zunger, D. M. Wood, "Electronic structure of LiZnN: Interstitial insertion rule," Phys. Rev. B 32, 1386-1389 (1985).
[36] G.Jaiganesh, T.Merito Anto Britto, R.D. Ethiraj and G.Kalpana, "Electronic and structural properties of NaZnX(X=P,As,Sb) an Ab-initio study" J. Phys.: Condens. Matter 20, 085220 (8pp) (2008).
[37] T. Gruhn, "Comparative ab initio study of half-Heusler compounds for optoelectronic applications," Phys. Rev. B 82, 125210 (2010).
[38] D. Kieven, R. Klenk, S. Naghavi, C. Felser, T. Gruhn, "I-II-V half-Heusler compounds for optoelectronics: Ab initio calculations," Phys. Rev. B 81, 075208 (2010).
[39] R. Umamaheswari, M. Yogeswari, G. Kalpana, "Ab-initio Investigation of Half-Metallic Ferromagnetism in half-Heusler Compounds XYZ (X= Li, Na, K and Rb; Y= Mg, Ca, Sr and Ba; Z= B, Al and Ga)," J. Magn. Magnetic Materials, 350, 167-170, (2014)
[40] F. Birch, "Finite strain isotherm and velocities for single-crystal and polycrystalline NaCl at high pressures and 300 °K," J. Geophys. Res. 83, 1257-1268 (1978).

Figure Captions:

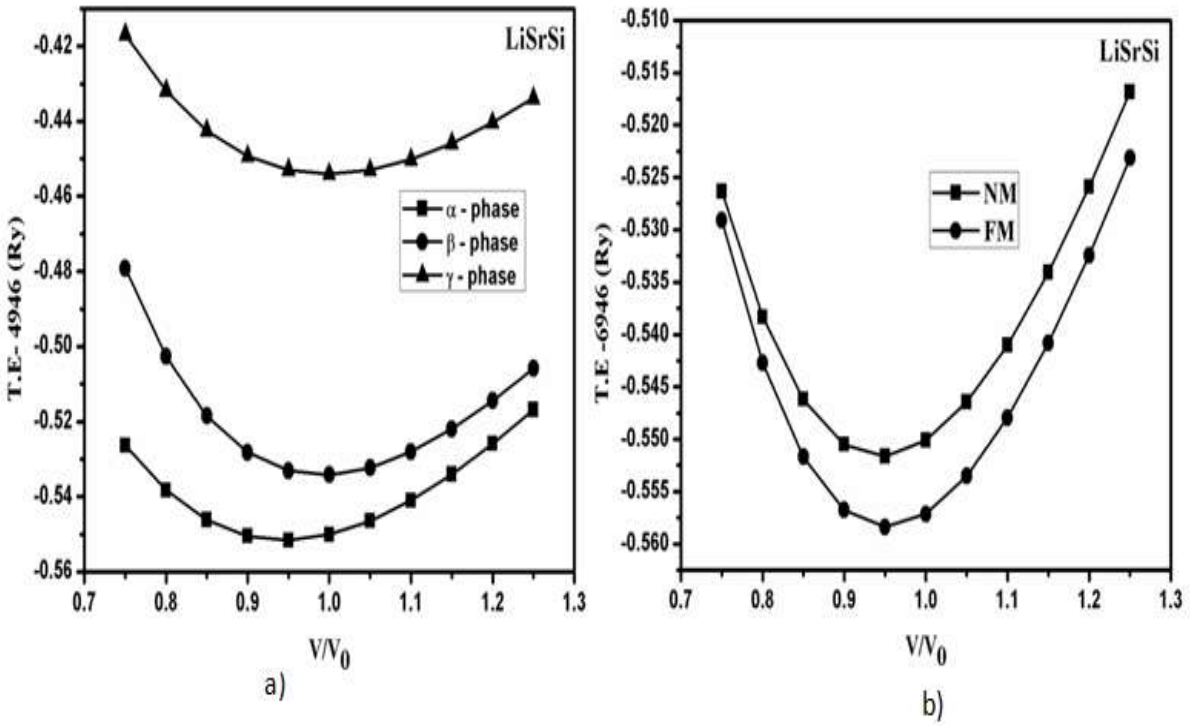

Figure 1: Plot showing the relationship between total energy per molecule and relative volume for (a) cubic α, β, and γ structures, and (b) non-magnetic (NM) and ferromagnetic (FM) states of the cubic α-structure of LiSrSi.

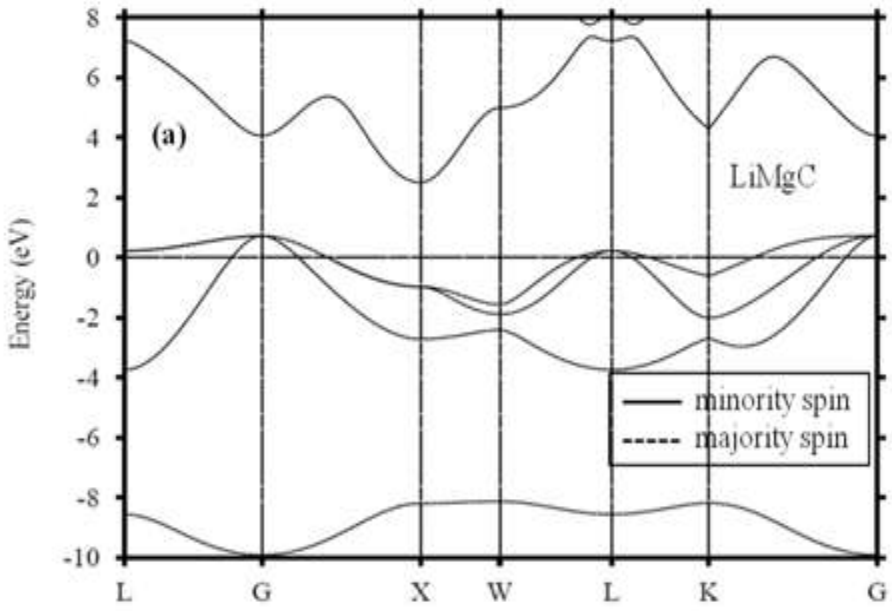

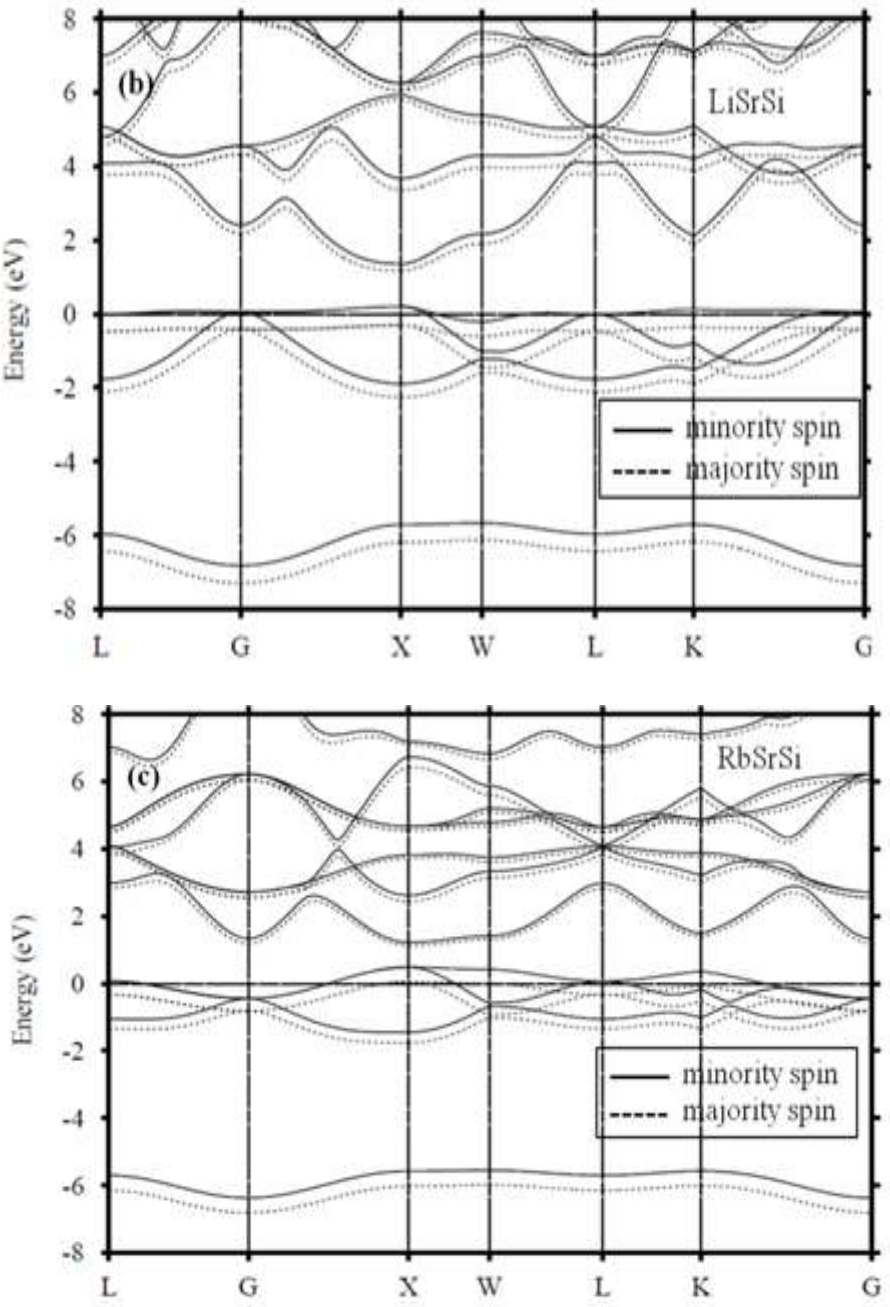

Figure 2: Spin-dependent electronic band structure for (a) LiMgC, (b) LiSrSi, and (c) RbSrSi compounds at their equilibrium volume. The Fermi level is established at zero.

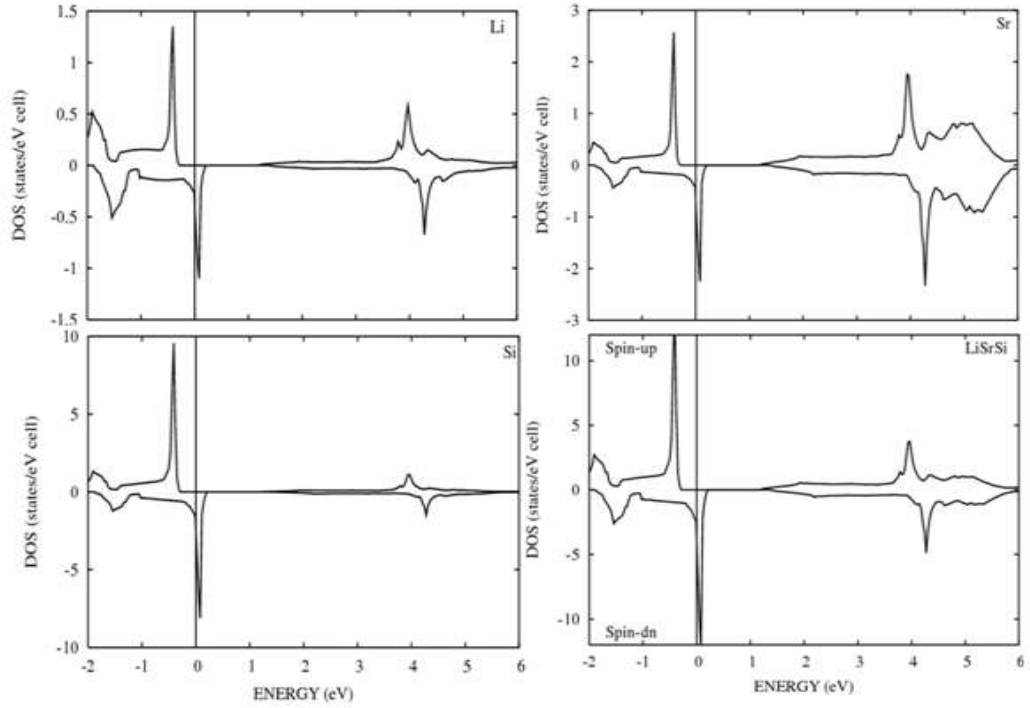

Figure 3: Spin-dependent density of states depicted as (a) total and (b) partial for LiSrSi at its equilibrium volume. The Fermi level is set at zero.

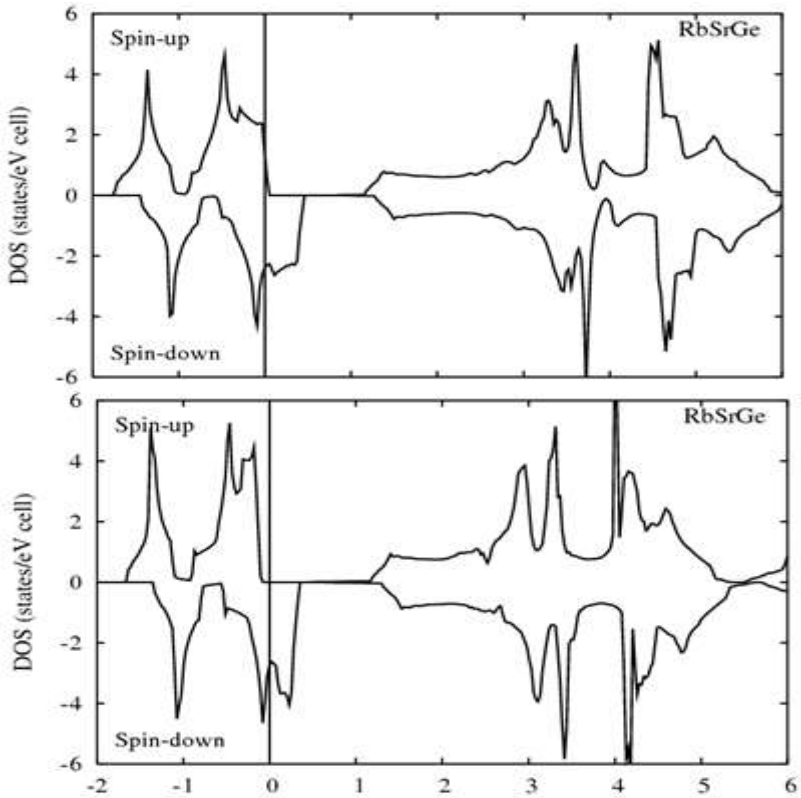

Figure 4: Spin-dependent total density of states for RbSrGe shown in (a) its equilibrium volume and (b) its expanded volume. The Fermi level is set to zero.

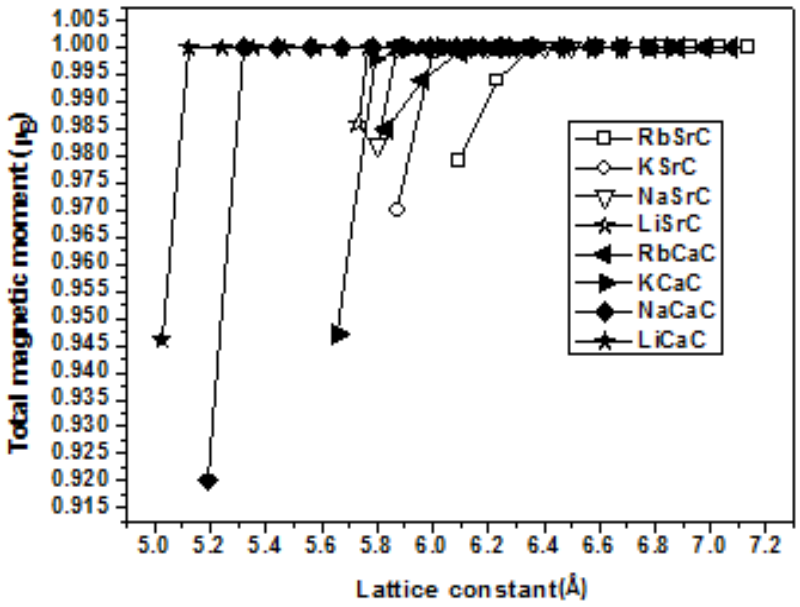

Figure 5: Graph illustrating the total magnetic moment (μ_B) with respect to lattice constant a (Å) for XYC compounds (X = Li, Na, K, and Rb; Y = Ca and Sr).

Table Captions:

Table 1: (a-d). Characteristics including lattice parameter (a) in Å, bulk modulus (B_0) in GPa, total energy difference ($\Delta E = E_{NM} - E_{FM}$) in meV, and Heat of formation (ΔH) in meV for (a) XYC, (b) XYSi, (c) XYGe, and (d) XYSn compounds.

Table 1 (a)

XYC	A		B_0		ΔE	ΔH
	NM	FM	NM	FM		
LiMgC	5.16	-	86.51	-	0	-9.20
NaMgC	5.60	5.60	67.00	66.36	53.62	-7.88
KMgC	6.08	6.12	40.92	42.60	139.61	-5.95
RbMgC	6.29	6.36	40.13	35.67	71.10	-5.64
LiCaC	5.64	5.66	52.69	55.60	146.7	-8.62
NaCaC	5.94	5.97	51.32	52.14	137.9	-7.84
KCaC	6.30	6.34 (6.56) [a]	30.20	30.71	61.98	-6.85
RbCaC	6.49	6.51	38.52	36.68	34.93	-5.91
LiSrC	5.83	5.95	21.31	35.80	17.53	-8.11
NaSrC	6.14	6.20	38.37	38.51	61.23	-7.83
KSrC	6.46	6.50	28.94	28.40	46.39	-7.14

RbSrC	6.73	6.74 (6.87) [b]	34.91	33.41	47.70	-6.12
LiBaC	6.25	-	44.90	-	0	-8.78
NaBaC	6.45	-	41.88	-	0	-8.49
KBaC	6.83	6.85	32.23	31.33	20.01	-7.98
RbBaC	7.10	7.09	21.05	21.32	57.48	-7.32

[a] Ref. [27]

[b] Ref. [28]

Table 1 (b)

XYSi	**A**		**B_0**		**ΔE**	**ΔH**
	NM	**FM**	**NM**	**FM**		
LiMgSi	6.15	-	45.48	-	0	-0.94
NaMgSi	6.49	-	39.84	-	0	-0.49
KMgSi	7.01	6.99	26.07	25.36	34.54	-0.22
RbMgSi	7.17	7.18	23.17	25.02	100.27	-0.21
LiCaSi	6.60	6.59	35.45	35.40	48.98	-0,83
NaCaSi	6.91	6.90	31.85	32.53	81.20	-0.44
KCaSi	7.30	7.30 (7.52) [a]	24.19	24.87	66.00	-0.32
RbCaSi	7.35	7.41	14.06	14.14	13.62	-0.28
LiSrSi	6.82	6.83	25.74	27.50	91.67	-0.85
NaSrSi	7.10	7.12	26.78	27.73	81.39	-0.62
KSrSi	7.47	7.51	23.30	22.62	38.00	-0.27
RbSrSi	7.54	7.58 (7.83) [b]	16.92	15.80	1.46	-0.09
LiBaSi	7.18	-	27.08	-	0	-1.37
NaBaSi	7.36	-	25.51	-	0	-1.44
KBaSi	7.74	-	21.87	-	0	-1.13
RbBaSi	7.89	-	19.50	-	0	-0.96

[a] Ref. [27]
[b] Ref. [28]

Table 1 (c)

XYGe	A		B_0		ΔE	ΔH
	NM	FM	NM	FM		
LiMgGe	6.17	-	43.31	-	0	-3.26
NaMgGe	6.52	-	37.59	-	0	-2.82
KMgGe	7.06	7.05 (7.22) [a]	25.20	24.53	18.61	-2.14
RbMgGe	7.23	7.24	22.34	23.91	92.76	-1.26
LiCaGe	6.63	6.62 (6.84) [a]	34.48	34.30	44.64	-3.05
NaCaGe	6.92	6.92 (7.16) [a]	30.58	31.29	72.86	-2.74
KCaGe	7.33	7.36 (7.58) [a]	23.82	24.41	60.79	-2.26
RbCaGe	7.37	7.43	12.94	13.05	2.95	-2.04
LiSrGe	6.85	6.87	25.44	27.22	84.88	-3.06
NaSrGe	7.11	7.14	25.92	26.77	76.42	-2.92
KSrGe	7.50	7.55	22.61	21.70	31.62	-2.51
RbSrGe	7.62	7.64 (7.88) [b]	18.11	16.78	4.47	-2.33
LiBaGe	7.22	-	26.69	-	0	-3.67
NaBaGe	7.39	-	24.83	-	0	-3.75
KBaGe	7.77	-	21.13	-	0	-3.53
RbBaGe	7.94	-	18.91	-	0	-3.27

[a] Ref. [27]
[b] Ref. [28]

Table 1 (d)

XYSn	A		B_0		ΔE	ΔH
	NM	FM	NM	FM		
LiMgSn	6.54	-	36.42	-	0	-1.22
NaMgSn	6.88	-	31.86	-	0	-0.91
KMgSn	7.37 (7.57) [a]	-	22.60	-	0	-0.42
RbMgSn	7.58	7.56	20.61	21.21	59.91	-0.38
LiCaSn	6.99 (7.23) [a]	6.99	29.32	29.13	3.76	-1.03
NaCaSn	7.30 (7.53) [a]	7.29	26.78	26.72	39.65	-0.80
KCaSn	7.70 (7.99) [a]	7.71	21.10	21.50	59.32	-0.49
RbCaSn	7.80	7.85	16.66	16.49	24.32	-0.29

LiSrSn	7.25	7.24	23.64	24.22	68.28	-1.10
NaSrSn	7.50	7.51	22.39	23.30	77.14	-0.99
KSrSn	7.87	7.91	19.83	19.73	44.31	-0.76
RbSrSn	7.97	8.00	16.00	15.03	3.156	-0.66
LiBaSn	7.55	-	23.47	-	0	-2.18
NaBaSn	7.73	-	21.94	-	0	-2.30
KBaSn	8.13	-	18.36	-	0	-1.75
RbBaSn	8.25	-	16.33	-	0	-1.73

[a] Ref. [27]

Table 2 (a-d): Comprehensive data encompassing total and partial magnetic moment in μ_B, Half-metallic gap (E_{HM}), majority spin band-gap ($E_g\uparrow$) in eV for XYZ compounds at their equilibrium volume, and critical lattice constant (a_{cr}) in Å for XYZ compounds.

Table 2(a)

XYC	M_X	M_Y	M_C	M_I	M_{TOT}	E_{HM}	E_g	a_{cr}
NaMgC	0.06	0.07	0.87	-0.01	1.0	0.16	2.0	4.78
KMgC	0.06	0.04	0.91	-0.01	1.0	0.33	0.93	5.44
RbMgC	0.08	0.05	0.88	-0.01	1.0	0.11	0.34	6.00
LiCaC	0.07	0.11	0.82	-0.01	1.0	0.54	2.27	5.03
NaCaC	0.06	0.10	0.85	-0.01	1.0	0.48	2.00	5.19
KCaC	0.07	0.08	0.87	-0.02	1.0	0.25 (0.38) [a]	1.44	5.79
RbCaC	0.05	0.05	0.93	-0.04	1.0	0.10	0.82	5.83
LiSrC	0.08	0.13	0.79	-0.01	1.0	0.18	2.08	5.73
NaSrC	0.05	0.11	0.85	-0.02	1.0	0.27	1.42	5.80
KSrC	0.05	0.10	0.87	-0.03	1.0	0.20	1.25	5.87
RbSrC	0.04	0.08	0.92	-0.04	1.0	0.13 (0.31) [b]	0.53(1.05) [b]	6.23
KBaC	0.03	0.10	0.90	-0.04	1.0	0.07	0.48	6.52
RbBaC	0.04	0.10	0.88	-0.03	1.0	0.12	0.25	6.46

[a] Ref. [27]
[b] Ref. [28]

Table 2 (b)

XYSi	M_X	M_Y	M_{Si}	M_I	M_{TOT}	E_{HM}	E_g	a_{cr}
KMgSi	0.08	0.14	0.74	0.02	1.0	0.09	1.11	5.97
RbMgSi	0.10	0.14	0.73	0.02	1.0	0.32	0.75	6.55
LiCaSi	0.09	0.16	0.69	0.03	1.0	0.14	1.19	5.51
NaCaSi	0.08	0.17	0.72	0.01	1.0	0.27	1.26	5.92
KCaSi	0.07	0.15	0.75	0.01	1.0	0.19 (0.29) [a]	1.13	6.83
RbCaSi	0.10	0.16	0.73	0.01	1.0	0.00	1.08	7.31

LiSrSi	0.10	0.16	0.70	0.03	1.0	0.30	1.47	6.26
NaSrSi	0.08	0.16	0.72	0.02	1.0	0.26	1.38	6.54
KSrSi	0.07	0.15	0.75	0.01	1.0	0.10	1.13	7.26
RbSrSi	0.08	0.14	0.68	0.00	0.91	- (0.14) [b]	- (0.94) [b]	7.68

[a] Ref. [27],
[b] Ref. [28]

Table 2 (c)

XYGe	**M_X**	**M_Y**	**M_{Ge}**	**M_I**	**M_{TOT}**	**E_{HM}**	**$E_g\uparrow$**	**a_{cr}**
KMgGe	0.09	0.15	0.72	0.03	1.0	0.02 (0.02) [a]	0.50	6.001
RbMgGe	0.13	0.19	0.66	0.02	1.0	0.015	0.34	6.630
LiCaGe	0.12	0.18	0.66	0.04	1.0	0.12 (0.03) [a]	1.25	5.531
NaCaGe	0.09	0.18	0.70	0.02	1.0	0.23 (0.19) [a]	1.28	6.004
KCaGe	0.09	0.16	0.72	0.02	1.0	0.16 (0.28) [a]	1.15 (1.21) [a]	6.924
RbCaGe	0.09	0.16	0.66	0.01	0.93	-	-	7.457
LiSrGe	0.12	0.17	0.67	0.04	1.0	0.28	1.52	6.296
NaSrGe	0.09	0.17	0.71	0.03	1.0	0.23	1.38	6.634
KSrGe	0.09	0.16	0.73	0.01	1.0	0.07	1.00	7.309
RbSrGe	0.07	0.15	0.070	0.00	0.94	- (0.12) [b]	- (0.90) [b]	7.709

[a] Ref. [27]
[b] Ref. [28]

Table 2 (d)

XYSn	**M_X**	**M_Y**	**M_{Sn}**	**M_I**	**M_{TOT}**	**E_{HM}**	**$E_g\uparrow$**	**a_{cr}**
RbMgSn	0.09	0.15	0.72	0.04	1.0	0.16	0.43	6.73
LiCaSn	0.07	0.12	0.38	0.03	0.58	-	-	8.63
NaCaSn	0.10	0.22	0.65	0.03	1.0	0.10 (0.08) [a]	1.13	6.18
KCaSn	0.09	0.18	0.69	0.03	1.0	0.21 (0.27) [a]	1.19 (1.23) [a]	7.16
RbCaSn	0.11	0.18	0.68	0.02	1.0	0.03	1.11	7.72
LiSrSn	0.12	0.18	0.64	0.05	1.0	0.21	1.38	6.53
NaSrSn	0.10	0.19	0.67	0.03	1.0	0.26	1.37	6.87
KSrSn	0.09	0.17	0.70	0.03	1.0	0.09	1.16	7.66
RbSrSn	0.08	0.15	0.61	0.02	0.87	-	-	8.10

[a] Ref. [27]

Table 3: Details featuring lattice constant (a_{ex}) in Å, total magnetic moment in μ_B, half-metallic gap (E_{HM}) in eV, and majority spin band-gap ($E_g\uparrow$) in eV for LiCaSn, RbCaGe, and RbSrZ (Z = Si - Ge) compounds at the expanded volume.

XYZ	a_{ex} (Å)	M_{TOT} (μB)	E_{HM} (eV)	$E_g\uparrow$ (eV)
LiCaSn	8.740	1.0	0.024	0.320
RbCaGe	7.572	1.0	0.018	0.894
RbSrSi	7.680	1.0	0.033	1.028
RbSrGe	7.868	1.0	0.030	0.591
RbSrSn	8.179	1.0	0.010	0.960

Table 4: Summarized magnetic properties of XYZ compounds within the half-Heusler structure. An entry of '–' signifies non-magnetic characteristics, '+' designates half-metallic ferromagnets (HMFs) at their optimized volume, and 'Δ' indicates HMFs at their expanded volume.

	C	Si	Ge	Sn	C	Si	Ge	Sn
LiMg	-	-	-	-	LiSr	+	+	+
NaMg	+	-	-	-	NaSr	+	+	+
KMg	+	+	+	-	KSr	+	+	+
RbMg	+	+	+	+	RbSr	+	Δ	Δ
LiCa	+	+	+	Δ	LiBa	-	-	-
NaCa	+	+	+	+	NaBa	-	-	-
KCa	+	+	+	+	KBa	+	-	-
RbCa	+	+	Δ	+	RbBa	+	-	-